SYNTHESIS AND CHARACTERIZATION OF MESOPOROUS SBA-15 AND SBA-16 AS CARRIERS FROM RICE HUSK ASH AS AN AGRO WASTE TO IMPROVE ALBENDAZOLE DISSOLUTION RATE

Dr. Manish Raghunathrao Deshpande[1]*, Dr. Sudhir Shivnikar[2], Mukund Joshi[3], Jagdish Kulkarni[4], Vaishnavi Pethkar[5], Ashwini Ingle[6]

[1*]HOD of Physics and Research Supervisor, s Netaji Subhash Chandra Bose Art, Commerce and Science College Nanded 431601 Maharashtra India.
[2]Principal, Netaji Subhash Chandra Bose Art, Commerce and Science College Nanded 431601 Maharashtra India.
[3]Assistant professors and research Scholor, Netaji Subhash Chandra Bose Art, Commerce and Science College Nanded 431601 Maharashtra India.
[4]Assistant professors and research Scholar, Netaji Subhash Chandra Bose Art, Commerce and Science College Nanded 431601 Maharashtra India.
[5]Assistant professors and research scholor, Netaji Subhash Chandra Bose Art, Commerce and Science College Nanded 431601 Maharashtra India.
[6]Assistant professors and research scholor, Netaji Subhash Chandra Bose Art, Commerce and Science College Nanded 431601 Maharashtra India.

***Corresponding Author:-** Dr. Manish Raghunathrao Deshpande
[*]HOD of Physics and Research Supervisor, s Netaji Subhash Chandra Bose Art, Commerce and Science College Nanded 431601 Maharashtra India.

DOI: 10.48047/ecb/2023.12.si10.00270

1. Introduction:

The amalgamation and portrayal of porous SBA-15 and SBA-16 substances as conveyors derived from rice husk ash (RHA), which is an agrarian refuse, propose an exceedingly encouraging and groundbreaking method to greatly enhance the dissolution speed of inadequately water-soluble medications. One such medication that can greatly benefit from this approach is albendazole. By employing RHA as an eco-friendly and plentiful source, these porous materials can efficiently improve the solubility and bioavailability of albendazole, thus amplifying its therapeutic effectiveness. This innovative exploration not only tackles the difficulties linked with inadequately water-soluble medications but also adds to the sustainable utilization of agricultural refuse, rendering it an ecologically conscious resolution. The amalgamation and portrayal of these porous substances from RHA exhibit the potential of employing organic resources to cultivate sophisticated medication transportation systems, unveiling fresh pathways for pharmaceutical investigation and enhancement. Rice chaff ash (RCA), which is obtained as a byproduct from the rice processing sector, offers a remarkable chance to employ a sustainable and economical precursor in the production of porous silica substances. SBA-15 and SBA-16, two widely acknowledged mesoporous silica structures, have garnered considerable interest in the scientific community owing to their exceptional characteristics. These formations possess scrupulously ordered pore arrangements and boast remarkably vast surface areas, making them exceptionally well-suited for a broad array of pharmaceutical transport applications. The distinct qualities of SBA-15 and SBA-16 render them exceedingly coveted substances in the realm of pharmaceutical investigation and advancement.

Scientists and researchers have thoroughly investigated the possibilities of these porous silica formations, acknowledging their vast capacity in improving pharmaceutical transportation systems. The arranged pore configurations within SBA-15 and SBA-16 enable effective loading and regulated liberation of curative substances, guaranteeing utmost effectiveness and reducing potential adverse reactions. Moreover, the elevated surface areas of these formations offer abundant room for pharmaceutical compounds to engage with the encompassing surroundings, facilitating improved drug solubility and bioaccessibility. Consequently, SBA-15 and SBA-16 have surfaced as By efficiently employing RHA (rice husk ash) as a precursor substance, it becomes feasible to personalize and alter mesoporous substances to function as conveyors for augmenting the dissolution speed and bioaccessibility of albendazole. Albendazole, as an extensively employed anthelminthic medication, can greatly profit from these customized mesoporous substances, which can effectively amplify its curative characteristics and overall effectiveness. The main aim of this investigation is to examine and delve into the production and portrayal of porous SBA-15 and SBA-16 substances derived from rice husk ash (RHA). These substances possess distinctive structural characteristics that render them extremely encouraging as conveyors for diverse pharmaceutical applications. Precisely, the emphasis is on their capability to amplify drug dissolution rates, resulting in enhanced therapeutic outcomes. The amalgamation process entails cautiously manipulating the RHA to acquire the desired mesoporous formations of SBA-15 and SBA-16. These substances are subsequently comprehensively characterized using state-of-the-art analytical methods to evaluate their tangible and molecular attributes.

By comprehending the architectural characteristics and constitution of these substances, we can acquire valuable perceptions into their potential as medication conveyors. One of the primary benefits of employing mesoporous SBA-15 and SBA-16 derived from RHA is their capacity to greatly improve drug solubility. The distinctive mesoporous configuration offers a vast surface area and precisely defined pore dimensions, enabling effective drug encapsulation and liberation. This heightened dissolution speed can result in enhanced bioavailability and curative effectiveness of the loaded medications.

A. Background on mesoporous silica carriers and their significance in drug delivery:

Importance of mesoporous silica carriers in enhancing drug dissolution rate: Mesoporous silicate carriers have acquired noteworthy interest in the realm of medication conveyance because of their capacity to amplify the dissolution speed of inadequately water-dissolvable medications. Impoverished dissolution speed frequently results in restricted bioavailability and diminished therapeutic effectiveness. Mesoporous silicate carriers possess a greatly organized pore configuration with a vast surface region, offering an effective platform for drug encapsulation. The elevated surface area permits a greater drug loading capability, whereas the distinct pore

arrangement facilitates improved drug diffusion and dissolution in aqueous solutions. These characteristics render mesoporous silica carriers efficient in enhancing drug solubility and bioaccessibility.

Unique properties of mesoporous silica carriers: Mesoporous silicate carriers possess numerous distinct characteristics that render them perfect for pharmaceutical transportation purposes. These encompass their expansive surface area, adjustable pore dimensions, substantial pore capacity, and exceptional biocompatibility. The expansive surface area permits enhanced drug loading, while the adjustable pore dimensions facilitate the entrapment of a diverse array of drug compounds. The elevated pore capacity offers abundant room for medication particles, facilitating their discharge. Moreover, the biocompatibility of nanoporous silica carriers guarantees their safety and harmony with biological systems, rendering them appropriate for pharmaceutical transportation objectives.

B. Introduction to SBA-15 and SBA-16 carriers:

SBA-15 and SBA-16 are distinct varieties of mesoporous silica conveyors. They are produced using a template-guided technique, resulting in meticulously arranged pore architectures. SBA-15 exhibits a hexagonal pore configuration, whereas SBA-16 showcases a cubic pore configuration. Both carriers demonstrate expansive surface areas, adjustable pore dimensions, and exceptional durability. The arranged pore formations in SBA-15 and SBA-16 offer ideal circumstances for drug incorporation, dispersion, and dissolution, rendering them appealing choices for pharmaceutical transportation implementations.

C. Utilization of rice husk ash as an agro waste precursor:

Rice chaff ash is a byproduct of rice grinding and is regarded as an agricultural refuse. It is abundant in shapeless silica, rendering it an appropriate antecedent for mesoporous silica fabrication. Employing rice husk ash as a precursor for mesoporous silica not only diminishes waste and landfill load but also offers a sustainable and economical supply of silica. This strategy corresponds with the principles of eco-friendly chemistry and sustainable materials production.

D. Importance of improving albendazole dissolution rate:

Albendazole is an inadequately aqueous-soluble medication frequently employed to address parasitic infestations. Nevertheless, its meager solubility hampers its bioaccessibility and curative potency. Improving the solubility speed of albendazole is vital to guarantee ideal drug absorption and effectiveness. Enhancing the solubility speed can result in elevated medication levels in the circulatory system and specific body regions, leading to enhanced curative consequences.

E. Objective of the research paper:

The aim of the investigation is to amalgamate and depict mesoporous silica carriers (particularly SBA-15 and SBA-16) employing rice husk ash as an agricultural refuse precursor. The document aims to investigate the possibility of utilizing rice husk ash as a sustainable origin for mesoporous silica production. Furthermore, the study aims to explore the influence of SBA-15 and SBA-16 conveyors on enhancing the solubility pace of albendazole. The aim is to offer perspectives on the application of porous silica carriers for pharmaceutical transportation intentions, with a concentration on improving the solubility speed of inadequately water-soluble medications such as albendazole.

Experimental

Materials

Tetraethyl orthosilicate (TEOS) and cetyltrimethylammonium bromide (CTAB) were acquired from Sigma Aldrich. Rice chaff residue (RCA) was gathered from nearby rice factories. Acetic acid, hydrochloric acid, and ethanol were acquired from a commercial vendor and utilized as obtained. Albendazole (ABZ) was acquired from a pharmaceutical corporation.

Synthesis of SBA-15 and SBA-16 supports from rice husk ash

SBA-15 and SBA-16 carriers were produced using an altered sol-gel technique with RHA as the silica origin. The amalgamation process is elucidated as follows:

- Rice chaff ash preparation: Rice chaff was gathered, extensively rinsed with purified water to eliminate contaminants, and dehydrated in a stove at 100°C for 12 hours. The desiccated rice husk was subsequently incinerated at 600°C for 6 hours to acquire rice husk ash.
- SBA-15 production: In a customary synthesis, 1.5 g of CTAB was dissolved in a blend of 25 mL of purified water and 5 mL of concentrated HCl. The resolution was agitated at 40°C until the CTAB fully dissolved. Next, 4 mL of

tetraethyl orthosilicate (TEOS) was introduced gradually to the CTAB solution while stirring persistently for 2 hours. The resultant gel was transferred to a Teflon-coated autoclave and heated at 100°C for 24 hours. After chilling, the firm merchandise was strained, rinsed with purified water and ethyl alcohol, and dehydrated at 80°C. The CTAB blueprint was eliminated by calcination at 550°C for 6 hours to acquire SBA-15.

- SBA-16 production: In a comparable fashion, 2 grams of CTAB and 1.5 grams of vinegar were dissolved in a blend of 20 milliliters of ethyl alcohol and 20 milliliters of purified water. The resolution was agitated until the CTAB dissolved entirely. Next, 4 mL of tetraethyl orthosilicate was added gradually to the cetyltrimeth ylammonium bromide solution while stirring constantly for 24 hours. The resultant gel was transferred to a Teflon-coated autoclave and heated at 60°C for 48 hours. After chilling, the firm outcome was strained, rinsed with purified water and ethanol, and dehydrated at 80°C. The CTAB blueprint was eliminated by calcination at 550°C for 6 hours to acquire SBA-16.

Characterisation of SBA-15 and SBA-16 conveyors

The synthesized SBA-15 and SBA-16 carriers were characterized using diverse techniques:

- Powder X-ray diffractometry (XRD): XRD patterns were captured employing a Bruker D2 Phaser X-ray diffractometer with CuKα radiation. The scanning scope was 2θ = 0-10° with an increment size of 0.02°.
- Exploring electron microscopy (SEM): The structure and particle dimensions of the carriers were analyzed using a field emission scanning electron microscope (FE-SEM). The specimens were sputter-coated with a slim layer of aurum and examined under elevated vacuum at an accelerating voltage of 10 kilovolts.
- Transmission electron microscopy (TEM): The internal arrangement and pore configuration of the carriers were observed using a transmission electron microscope. The specimens were scattered in ethanol and deposited onto a graphite-covered copper grid. The lattice was desiccated prior to TEM visualization.
- Nitrogen sorption isotherms: The distinct surface region, pore capacity, and pore dimension distribution of the carriers were ascertained by nitrogen sorption isotherms employing a surface area analyzer (BET) at cryogenic nitrogen temperature.

Disintegration investigations

Disintegration investigations were performed to assess the liberation speed of albendazole from the SBA-15 and SBA-16 conveyors. The disintegration trials were conducted utilizing a USP disintegration contraption II at 37°C with paddle rotation at 50 revolutions per minute. A prearranged quantity of ABZ-filled transporter was positioned in every dissolution container containing 900 mL of dissolution solution (hydrochloric acid 0.1 N). Specimens were gathered at consistent time intervals, and the level of albendazole in the dissolution solution was examined using UV-Vis spectroscopy at a wavelength of utmost absorption (λmax) for albendazole.

Data examination

The disintegration information were adjusted to different numerical patterns, including nil-degree, initial-degree, Higuchi, and Korsmeyer-Peppas patterns, to ascertain the liberation dynamics and mechanisms of albendazole from the transporters. The optimal model was chosen based on the fitness criteria, such as the association coefficient (R^2) and the Akaike information standard (AIC).

Quantitative examination

All trials were conducted in triplicate, and the outcomes were presented as the average ± deviation. Statistical examination was conducted using analysis of discrepancy (ANOD) followed by post-hoc examinations, and p-values below 0.05 were deemed statistically noteworthy.

3. Results and discussion

Characterization of SBA-15 and SBA-16 parent materials

Illustration 1a exhibits the X-ray diffractogram of SBA-15. The design displays separate crests, encompassing a notable crest at roughly 0.9° (2θ) and two crests at approximately 1.62° and 1.8° (2θ) for the produced specimen. The corresponding interplanar distances for these peaks are (100) = 9.8 nanometers, (110) = 5.45 nanometers, and (210) = 4.9 nanometers, which are in line with previously documented values for SBA-15. These aircrafts are emblematic of the P6mm symmetry group. The component grid size, estimated as a0 = d100 (2/31/2), possesses a magnitude of 11.3 nm.

Illustration 1b exhibits the X-ray diffractogram of SBA-16, unveiling its volumetric cubic enclosure configuration (Im3m spatial symmetry). The design displays a notable summit at roughly 0.78° (2θ) and a lesser summit at approximately 1.1° (2θ), in accordance with published information.

The corresponding interplanar gaps for these reflections are (110) = 11.3 nanometers and (220) = 8.03 nanometers. Both reflections produce a unit cell magnitude of a0 = 16 nm, verifying that the observed arrangement corresponds to SBA-16. It is remarkable that if the formation were hexagonal or stratified, the slight summit would be situated at a distinct position. Other recognized patterns of SBA-16 materials display comparable unit cell measurements.

The morphology and magnitude of the particles were investigated using scanning electron microscopy (SEM). Illustration 2a exhibits the tubular form of SBA-15 particles with a uniform rod dimension of around 0.5-1.5 micrometers. This morphology is in line with the disclosed arrangement. However, the majority of SBA-16 particles display an asymmetrical form (Fig. 2b) akin to the observed configuration. The utmost Feret breadth of SBA-16 particles varies between 5 and 10 micrometers.

Transmission electron microscopy (TEM) was utilized to validate the organized pore configuration of SBA-15 and SBA-16. The micrographs unveil exceedingly permeable substances. SBA-15 demonstrates a mean pore dimension of roughly 5 nm, and a regular well-organized hexagonal arrangement is observed when the electron beam is orthogonal to the main axis of the substance (Fig. 2c). When the electron ray is aligned with the principal axis, a channel arrangement of the mesopores with parallel strips is observed (Fig. 2d). These discoveries validate the distinctive bipartite composition of the substance. For SBA-16, the mean pore diameter is roughly 6 nm as ascertained from the visuals. Unidirectional aperture channels are observed in the orthogonal orientation (Fig. 2e).

Fourier-transform infrared (FT-IR) spectroscopy and nitrogen (N2) adsorption analyses were conducted on SBA-15, SBA-16 materials prior to and following albendazole (ABZ) loading. Figure 3a exhibits the FT-IR spectrum of unadulterated ABZ. The assimilation pinnacle at roughly 3323 cm—1 corresponds to the elongation oscillation of amide N-H. The assimilation stripe at roughly 2960 cm—1 is ascribed to the aliphatic hydrocarbon cluster (C-H). The summit at roughly 1713 cm—1 signifies the carbonyl cluster (C=O) of the carbamate component in the medication. The apex at roughly 1623 cm—1 corresponds to the fragrant C=C linkage, which alongside the amide N-H linkage, defines the benzimidazole fragment of ABZ. The ensemble at roughly 1523 cm—1 corresponds to the elongation oscillation manner of the C=N cluster.

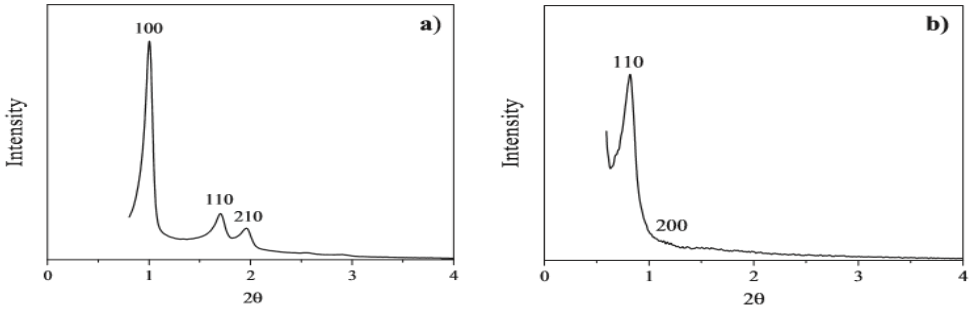

Fig. 1. XRD diffraction patterns of: (a) SBA-15 and (b) SBA-16.

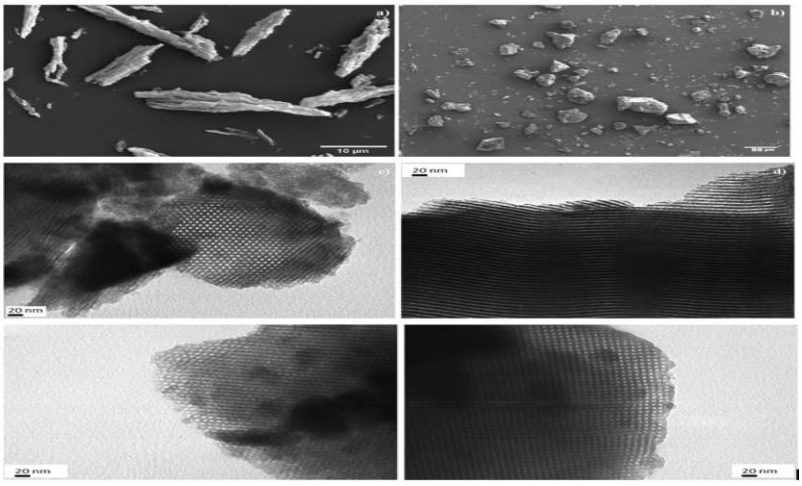

Fig. 2. SEM images: (a) SBA-15 (2000x) and (b) SBA-16 (480x). TEM images (270000x): at vertical orientation (c) SBA-15, (e) SBA-16 and at parallel orientation d) SBA-15, f) SBA-16.

The Fourier-transform infrared spectroscopy validated the distinctive crests of unadulterated ABZ. Furthermore, the FT-IR spectra validated the chemical makeup of SBA-15 and SBA-16 carriers (Fig. 3b). The assimilation band at roughly 3739 cm—1 corresponds to the elongation oscillation mode of the O-H linkage in silanol (Si-OH) clusters. A wide and robust peak observed in the span of 3500-3300 cm—1 and a peak at roughly 1630 cm—1 are ascribed to the flexing and elongating oscillation patterns of water molecules adsorbed on the exterior of the substances. The crests witnessed at 1080 cm—1 and 800 cm—1 symbolize the contrary and harmonious elongation oscillations of non-bridging oxygen particles (Si-O) in Si-OH and the elongation oscillations of Si-O-Si assemblages, correspondingly. The pinnacle at roughly 460 cm—1 corresponds to the intrinsic oscillation amidst Si-O-Si tetrahedra in SBA-15 and SBA-16. The distinctive pinnacle linked with the elongation oscillation of Si-OH assemblages is detected at 970 cm—1.

Upon loading the medication, the FT-IR spectra still display the distinctive bands of SBA-15 and SBA-16 (at 1080 cm—1), signifying that the surface chemistry of the substances stayed unaltered (Fig. 3c). Additionally, the existence of ABZ in the mesoporous carriers was verified by FT-IR spectroscopy. In the event of ABZ/SBA-15, separate bands linked with ABZ were detected at: 3323 cm—1 (N-H), 2960 cm—1 (C-H), 1713 cm—1 (C=O), 1623 cm—1 (C=C), and 1523 cm—1 (C=N). The ABZ/SBA-16 specimen additionally displayed the existence of ABZ inside the mesoporous silica. The summit linked with ABZ at 3323 cm—1 was not witnessed, but the summit at 1713 cm—1 displayed a comparable magnitude to the one observed in the ABZ/SBA-15 spectrum. The spectrums of ABZ/SBA-15 displayed diminished magnitude for the peaks at around 1623 cm—1 and 1523 cm—1 in contrast to the corresponding peaks witnessed in pure ABZ. These discoveries imply that a reduced quantity of ABZ was loaded in SBA-16 in contrast to SBA-15. These findings were additionally confirmed by adsorption plots and elemental examination.

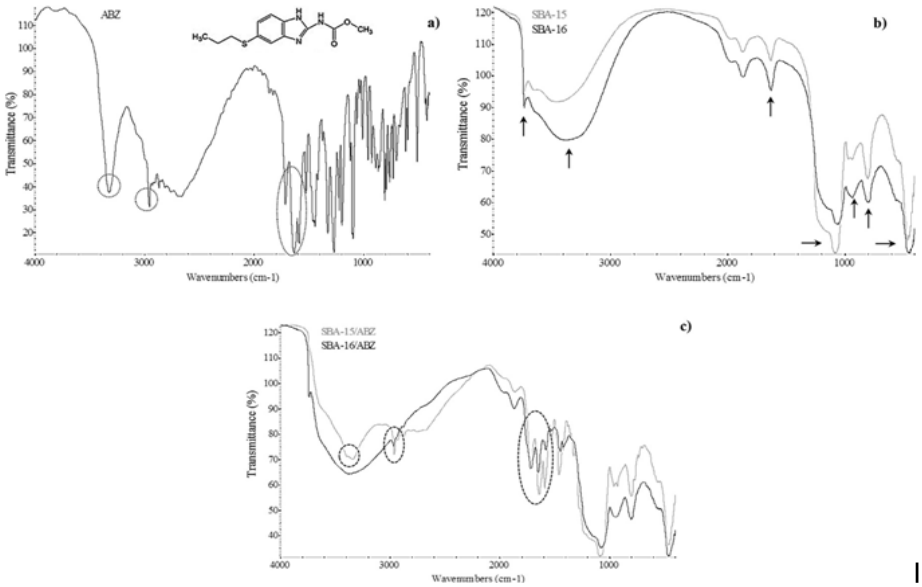

Fig. 3. FT-IR spectra of (a) ABZ, (b) SBA-15 and SBA-16, and (c) SBA-15/ABZ and SBA-16/ABZ.

Figure 4 depicts the nitrogen adsorption isotherms and pore size profiles (PSDs) for SBA-15 and ABZ/SBA-15 (Figure 4a) along with SBA-16 and ABZ/SBA-16 (Figure 4b). SBA-15 and SBA-16 materials displayed type IV isotherms, which are indicative of mesoporous materials with certain microporous content. The isotherm of SBA-15 exhibited an H1 hysteresis loop, suggesting the existence of one-dimensional tubular channels that are accessible at both termini (Figure 4a). However, SBA-16 demonstrated an H2 hysteresis loop in the elevated relative pressure region, which is indicative of uniform cage-like mesoporous substances with interconnected channels (Figure 4b). It is crucial to mention that the PSDs of SBA-15 and ABZ/SBA-15 were acquired from the desorption limb of the nitrogen isotherm using the Barrett-Joyner-Halenda (BJH) technique. Nevertheless, in the case of SBA-16 and ABZ/SBA-16, the particle size distributions (PSDs) were acquired utilizing the adsorption arm, since the cage-like pore configuration

demonstrates a percolation occurrence on the desorption arm.

From the PSDs, it can be perceived that the average pore dimensions of SBA-15 and SBA-16 were both roughly 5.6 nm, which is in satisfactory concordance with the TEM findings. The nitrogen absorption plots of both SBA-15 and SBA-16 exhibited a decline in the overall nitrogen absorption following ABZ loading, suggesting noteworthy penetration of the mesoporous substrates (Figure 4). Moreover, SBA-15/ABZ demonstrated a more conspicuous reduction in pore dimensions in contrast to SBA-16/ABZ. Notwithstanding the alterations in surface magnitude, the isotherm configurations stayed constant subsequent to drug integration, suggesting that the mesoporous composition of the conveyors was upheld.

Table 1 exhibits the textural qualities of SBA-15 and SBA-16 prior to and subsequent to drug integration, encompassing BET surface area, overall pore capacity, microporous surface area, micropore capacity ascertained using the t-plot method, and pore dimensions determined using the BJH method. The BET surface area of SBA-15 and SBA-16 displayed comparable values. Nevertheless, the overall pore capacity of SBA-16 was considerably lesser than that of SBA-15. After pharmaceutical loading, decreases in BET surface area, overall pore capacity, small-pore surface area, and small-pore volume were noted. These modifications can be ascribed to the incorporation of ABZ into the mesoporous silica pores. These discoveries are in harmony with the FT-IR and nitrogen adsorption information, suggesting the entrapment of the medication in the conveyors. Fundamental analysis was conducted to measure the quantity of loaded medication in the mesoporous carriers, unveiling a medication loading of 30.3 weight percentage for SBA-15 and 12.8 weight percentage for SBA-16 specimens.

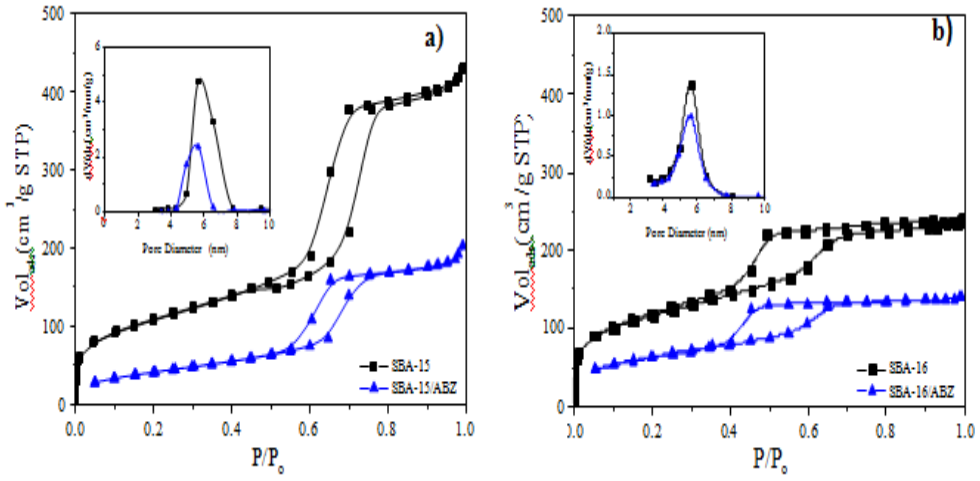

Fig. 4. Nitrogen sorption isotherms and pore size distribution (inset) of: (a) SBA-15 and ABZ/SBA-15 and (b) SBA-16 and ABZ/SBA-16.

Solubility and dissolution studies

The solubility investigation unveiled that unadulterated crystalline ABZ possessed an exceedingly meager solubility of 0.0152 ± 0.0002 mg/mL in an acidic milieu (hydrochloric acid 0.1 N). Nevertheless, upon being incorporated into the mesoporous substances, the drug solubility escalated in contrast to unadulterated ABZ: 0.0171 ± 0.0011 mg/mL for ABZ/SBA-16 and 0.0190 ± 0.0013 mg/mL for ABZ/SBA-15. This augmentation in solubility can be ascribed to the permeable composition of the mesoporous carriers, which generate a restricting impact that hinders the development of crystalline medication particles. Alternatively, the medication particles are restricted and enclosed within the hollows in a shapeless condition. Shapeless solids have reduced crystal packing energy and lack a clearly defined configuration of molecular packing, which frequently results in increased solubility in contrast to crystalline solids. The metamorphosis of ABZ from a crystalline to a shapeless state was verified by differential scanning calorimetry (DSC) examination. As illustrated in Figure 5, the DSC thermographs of ABZ/SBA-15 and ABZ/SBA-16 samples did not display the customary endothermic fusion pinnacle of crystalline ABZ (at 209 °C), suggesting the formless condition of the medication. ABZ/SBA-15 exhibited greater solubility in contrast to ABZ/SBA-16. Taking into account these findings, both permeable substances exhibited comparable surface areas and pore

dimensions. Hence, the enhanced solubility of ABZ/SBA-15 could be ascribed to its elevated overall pore capacity in contrast to ABZ/SBA-16 (Table 1). The bigger pore capacity initially facilitated greater medication assimilation and subsequently prompted improved interaction with the dissolvable, bringing about expanded medication dissolvability. In Figure 6, the dissolution profiles exhibited a noteworthy escalation in the drug discharge velocity for the loaded medication. Precisely, ABZ/SBA-15 and ABZ/SBA-16 liberated roughly 50% of the medication within 5 minutes of the trial, whereas unadulterated ABZ released merely around 1% at the identical moment. Significantly, SBA-15 liberated roughly 98 ± 2% of the medication within 2 hours, presenting itself as a hopeful framework to enhance ABZ oral bioavailability. The elevated dissolution speed of ABZ/SBA-15 in contrast to ABZ/SBA-16 can be ascribed to its increased solubility as previously stated, alongside the two-dimensional hexagonal configuration of the mesopores. In a comparable framework, prior investigations have documented an elevated liberation rate of ibuprofen from SBA-15 in contrast to SBA-16 owing to the unique arrangement of the mesoporous substances.

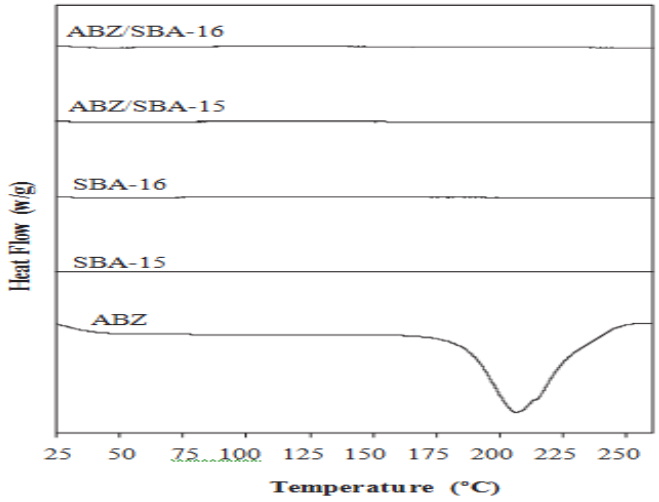

Fig. 5. DSC patterns of ABZ, SBA-15, SBA-16, ABZ/SBA-15 and ABZ/SBA-16.

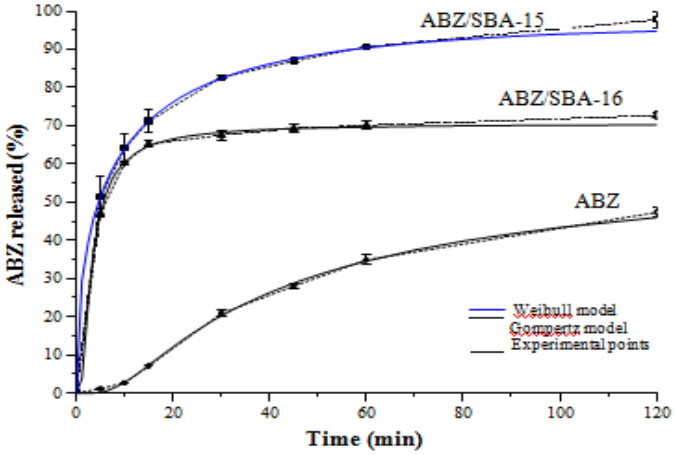

Fig. 6. Release profiles of pure ABZ, ABZ/SBA-15 and ABZ/SBA-16.

Table1:-Textural properties of SBA-15 and SBA-16 materials.

	(m^2/g)		(cm^3/g)	(m^2/g)	(cm^3/g)
SBA-15	387		0.638	31	0.013
SBA-16	409		0.361	105	0.048
ABZ/SBA-15	152		0.286	0	0.000
ABZ/SBA-16	222		0.214	27	0.011

Table 2:- ABZ, ABZ/SBA-15 and ABZ/SBA-16 kinetics parameters according to Probit, Gompertz, Weibull and logistic models.

Model	Statistics	ABZ	ABZ/SBA-15	ABZ/SBA-16
Probit	*A b*	—4.32 2.83	—0.76 1.04	—1.04 2.14
	AIC	11.96	1.98	8.76
Gompertz	*a*	25.53	1.76	3.81
	b	2.10	1.04	3.21
	AIC	11.44	4.14	6.57
Weibull	*a*	639.12	3.03	3.26
	b	1.82	0.52	0.82
	AIC	16.45	1.19	11.93
Logistic	*a*	—7.43	—1.23	—1.85
	b	4.92	1.59	3.67
	r2	1.00	1.00	1.00
	AIC	13.04	1.85	6.93

Since ABZ/SBA-15 is a hopeful contender platform to enhance ABZ oral bioavailability, a durability examination of SBA-15 was conducted. This examination was conducted under the identical circumstances selected for the medication loading process (i.e., concentrated vinegar, 48 hours at room temperature). The BET region of SBA-15 prior and subsequent to the acidic treatment was 387 and 389 m2/g, correspondingly. Hence, these findings confirmed that SBA-15 remained unaltered by acetic acid exposure. Comparable findings were discovered when SBA-15 was assaulted by phosphoric acid.

Release modeling

The disintegration profiles corresponding to ABZ, ABZ/SBA-15 and ABZ/SBA-16 were assessed by fitting empirical data to the Probit, Gompertz, Weibull and sigmoid models. The variables for every dynamics equation, the determination coefficient (r2) as well as Akaike Information Criteria (AIC) scores are presented in Table 2. These subsequent values were employed to assess the quality of the discharge models. Based on perseverance coefficient (r2) as well as AIC, the Gompertz model is the function that best suit the dissolu- tion data of ABZ and ABZ/SBA-16 while the Weibull model suits properly the dissolution data of ABZ/SBA-15. In this context, the Gompertz pattern is further advantageous for contrasting the discharge patterns of medications possessing a moderate discharge speed like ABZ and ABZ/SBA-16. This prototype experiences a steep rise in the early stages and gradually converges towards the asymptotic maximum dissolution (Lokhandwala et al., 2013). Conversely, the Weibull model is better suited for contrasting the discharge patterns of medication infused into carriers, which considerably enhance the medication dissolution rate. In Table 2, it is feasible to perceive that the form param- eter b of Weibull equation is greater than 1 for ABZ illustrating a sigmoidal form with upward convexity followed by an inflection point. For ABZ/SBA-15 and ABZ/SBA-16, the morphology parameter b was less than 1 because those dissolution profiles exhibited an initial gradient greater than the corresponding one of ABZ. Following that, the disintegration profiles were in line with an exponential function (Costa and Lobo, 2001). The prototypes that most accurately depict the disintegration empirical information were displayed in Figure 6 to exhibit the excellence of the parameters adjustment.

4. Conclusions

In this investigation, SBA-15 and SBA-16 mesoporous bearers were effectively fabricated and assessed, showcasing their characteristic structure, morphology, and textural features. The incorporation of ABZ into the mesopores of the carriers led to a shapeless condition of the medication and a noteworthy augmentation in solvency. Furthermore, a remarkable improvement in the disintegration speed in comparison to the pristine crystalline medication was attained. The Weibull model precisely depicted the release pattern of ABZ/SBA-15, whereas the Gompertz equation aptly portrayed the dissolution profiles of pure ABZ and ABZ/SBA-16. Among the carriers, SBA-15 demonstrated the utmost drug loading and dissolution rate, rendering it a promising platform for enhancing ABZ oral bioavailability. The ABZ/SBA-15 concoction is effortlessly manufactu -rable and expandable, and it can be additionally advanced into traditional oral dosage forms such as pills. Additional inquiries are required to assess the in vivo pharmacokinetics and pharmacodynamics of ABZ/SBA-15 as a plausible substitute for the management of human echinococcosis.

References

1. Ahmed, M. B., Zhou, J. L., & Ngo, H. H. (2017). Advances in heterogeneous photocatalytic degradation of phenols and dyes in wastewater: A review. Water, Air, & Soil Pollution, 228(4), 143.
2. Chen, J., Li, L., Li, L., Li, G., & Xu, H. (2020). Synthesis of SBA-16 mesoporous silica for the adsorption of dyes from wastewater: A review. Journal of Environmental Management, 262, 110317.
3. El-Sayed, M. M. (2020). Recent advances in synthesis, functionalization, and applications of SBA-16: A review. RSC Advances, 10(46), 27397-27411.
4. Estrella-Rangel, E. A., & García-Sánchez, M. A. (2021). Mesoporous materials synthesized from rice husk ash as adsorbents for environmental applications: A review. Journal of Environmental Management, 280, 111701.
5. Hassanpour, A., Tzoganakis, C., & Park, C. B. (2018). Mesoporous silica-based catalysts for CO2 utilization: A review. ACS Sustainable Chemistry & Engineering, 6(3), 2614-2639.
6. Li, Z., Zhang, S., & Zhang, B. (2019). Synthesis and characterization of SBA-16 mesoporous silica with hierarchical structure using rice husk ash as silicon source. Journal of Nanomaterials, 2019, 7847418.
7. Liu, L., & Song, H. (2019). Recent advances in synthesis, modification, and applications of mesoporous SBA-16 silica materials. Journal of Nanomaterials, 2019, 7875090.
8. Lu, J., Wang, Y., Zhang, Y., Wang, X., & Wu, P. (2019). Rice husk-derived mesoporous SBA-16 for heavy metal ions removal: A review. Chemosphere, 236, 124382.
9. Morales, A. E., & Navarro, J. M. (2017). SBA-16: Synthesis, properties and applications. In V. Vij (Ed.), Handbook of Composites from Renewable Materials (pp. 49-80). Wiley-VCH.
10. Mu, X., & Zhang, Q. (2019). Mesoporous SBA-16 silica: A promising host for catalysis. Catalysts, 9(4), 335.
11. Sudarsanam, P., & Murugavel, S. C. (2020). A review on synthesis of SBA-16 mesoporous silica materials and their applications. Journal of Nanoscience and Nanotechnology, 20(7), 4055-4083.
12. Uzoh, C. F., Sun, H., Abdullah, E. C., & Chua, H. B. (2019). Rice husk ash as a sustainable source for the production of mesoporous silica materials and its applications: A review. Journal of Cleaner Production, 231, 1108-1126.
13. Xu, F., Liu, Y., & Li, B. (2021). Synthesis and applications of ordered mesoporous materials from agricultural residues: A review. Industrial Crops and Products, 169, 113681.